Defraeye T., Verboven P., Nicolai B. (2013), CFD modelling of flow and scalar exchange of spherical food products: turbulence and boundary-layer modelling, *Journal of Food Engineering* 114 (4), 495-504.
http://dx.doi.org/10.1016/j.jfoodeng.2012.09.003

CFD modelling of flow and scalar exchange of spherical food products: turbulence and boundary-layer modelling

Thijs Defraeye [a, *], Pieter Verboven [a], Bart Nicolai [a,b]

[a] *MeBioS, Department of Biosystems, University of Leuven, Willem de Croylaan 42, 3001 Heverlee, Belgium*

[b] *VCBT, Flanders Centre of Postharvest Technology, Willem de Croylaan 42, 3001 Heverlee, Belgium*

Abstract

The performance of several steady Reynolds-averaged Navier-Stokes turbulence models and boundary-layer modelling approaches is evaluated for a single sphere, by comparison with empirical data for a Reynolds number range of 10 to $3.2x10^4$. A sphere serves here as a representative model for many spherical food products. The shear stress transport (SST) k-ω turbulence model performs exceptionally well when combined with low-Reynolds number modelling (LRNM) of the boundary layer, which confirms that the turbulence model characteristics are particularly suitable to deal with this specific flow problem. Especially the k-ε turbulence models are less accurate at higher Reynolds numbers (> 10^2). Boundary-layer modelling with wall functions (WFs) leads to inaccurate flow-field and scalar transfer predictions, compared to LRNM. However, LRNM grids and their inherently higher computational cost are often not practically feasible, leaving WFs as the only option. It is shown that using cell sizes on the sphere surface of a few millimetres, typical for CFD studies on food products, can compromise accuracy, and grids with smaller cell sizes are actually required.

Keywords: sphere, validation, cooling, convective heat transfer coefficient, heat, stack

[*] Corresponding author. Tel.: +32 (0)16321618; fax: +32 (0)16322966.

E-mail address: thijs.defraeye@biw.kuleuven.be

1. Introduction

In postharvest technology and food processing, computational fluid dynamics (CFD) is often applied as an alternative to experimental research (e.g., in wind tunnel, cool room or processing equipment; Ambaw et al., 2012a). For food products in particular, CFD is used, amongst others, for studies on convective cooling of produce (da Silva et al., 2010; Dehghannya et al., 2010; Martins et al., 2011; Tutar et al., 2009; Verboven et al., 1997, 2006; Zou et al., 2006), long-term storage of horticultural products (Ambaw et al., 2012b; Delele et al., 2008, 2009; Hoang et al., 2000, 2003; Nahor et al., 2005), convective drying of food (Kaya et al., 2006), oven design (Verboven et al., 2000a, 2000b, 2003) as well as individual quick freezing (Peralta et al., 2010).

The use of CFD for these applications has specific advantages: (i) No restrictions are imposed to the complexity of the model, in contrast to, e.g., wind-tunnel experiments; (ii) A very high spatial (and temporal) resolution can be obtained with respect to the flow field and scalar transfer (e.g., heat). Wind-tunnel or field tests often do not allow simultaneous measurements of relevant parameters at the same location, often have problems regarding accessibility within complex models, and measurements at high spatial resolution are not always straightforward and very time-consuming (Kondjoyan, 2006); (iii) Information of momentum and scalar transfer at surfaces is available (e.g., heat/mass fluxes). This is particularly relevant for determining the scalar exchange of the product with the environment and allows, due to the high resolution, to determine surface-averaged quantities (e.g., heat flow); (iv) No scaling issues (e.g., Reynolds number in wind-tunnel tests) are present as simulations can be performed at "full scale".

The accuracy of CFD simulations is however to a large extent determined by the applied numerical modelling approaches, and their validation is required. Particularly the choice of the turbulence modelling and boundary-layer modelling approach is important since they form the cornerstones of a CFD simulation and since a large variability is often found in their performance (e.g., Defraeye et al., 2010a, 2010b). Regarding turbulence modelling, steady Reynolds-averaged Navier-Stokes (RANS) is preferred in food engineering (Kondjoyan, 2006), compared to other (unsteady) approaches, such as large-eddy simulation (LES). The higher computational cost of LES, the higher grid resolution and the detailed knowledge required on the inlet conditions (Kondjoyan, 2006) make LES less interesting for food engineers, particularly when modelling large complex systems such as flow in stacks of food products. The accuracy of RANS, where all scales of turbulence are modelled by a turbulence model, is, however, usually less than with LES, since the large turbulent structures in the flow are explicitly resolved in the latter approach. Regarding boundary-layer modelling, wall functions (WFs) are often preferred over low-Reynolds number modelling (LRNM) for increased computational economy and easier grid generation: WFs, which model the flow quantities in the boundary-layer region by calculating them by means of semi-empirical functions, avoid resolving the boundary layer explicitly, which requires an extremely high grid resolution for LRNM at high Reynolds numbers. Thereby, LRNM is often not practically applicable for complex 3-D configurations (Kondjoyan, 2006). WFs however often lead to inaccurate predictions, especially for wall friction and convective heat transfer (e.g., Defraeye et al., 2010a). CFD modellers should acknowledge the impact of these different modelling approaches on the accuracy of their results, particularly since their choices are often driven by computational restrictions to time or resources, instead of modelling accuracy. Due to these restrictions, steady RANS with WFs is often considered the only option for efficient modelling of complex 3D systems, such as flow in stacks of food products.

With respect to modelling accuracy, predictions of flow and scalar transfer around a sphere are particularly relevant for postharvest technology and food processing since a sphere is a representative model system for many spherical food products (e.g., apple, tomato, peach, several berries, etc.) and thus a basic component in CFD studies of more complex configurations (e.g., products stacked in a container; Delele et al., 2008; Hu and Sun, 2001; Verboven et al., 1997, 2006). CFD has been applied in the past to model fluid flow around a single sphere (e.g., Constantinescu and Squires, 2004; Dhole et al., 2006; Dixon et al., 2011; Feng and Michaelides, 2000; Johnson and Patel, 1999). In these studies however: (1) mostly low to moderate Reynolds numbers (< 1000) were considered, which are less interesting for food engineering. The few studies performed at higher Reynolds numbers usually applied unsteady techniques, such as LES, which is feasible for fundamental fluid mechanics problems, but less interesting in large-scale biotechnology applications; (2) an intercomparison of different turbulence modelling and boundary-layer modelling approaches is often not provided, although very important for food engineering, due to the large variety of models available; (3) often, very few details of the computational grid are given, or the sensitivity to them is not investigated. These grid specifications are, however, very valuable when considering larger configurations, e.g., stacks.

This study aims at alleviating these issues to some extent. Thereto, the results of several RANS turbulence models and boundary-layer modelling approaches are compared with empirical data for flow and scalar transfer around a single sphere. A comparison of drag coefficient, Nusselt number, separation angle and recirculation length is performed. A Reynolds number range relevant for postharvest and food processing applications is evaluated. Heat is taken as the (passive) scalar to study convective transport. Apart from this CFD validation, the influence of grid size on the sphere surface is also investigated.

2. Materials and methods

2.1 Numerical model

A single sphere was considered, for which empirical flow-field data are readily available in literature. The inner structure of the sphere, and the heat or mass transport therein, were not modelled since the focus was on air-side flow and scalar transfer. The diameter of the sphere (D) is 75 mm, which is a representative size for, e.g., an apple. Based on symmetry, the computational model of the sphere was reduced by a factor 4. The computational domain is presented in Figure 1. The blockage ratio, which is the ratio of the frontal area of the sphere to the surface area of the inlet of the computational domain, is 0.6%, which is sufficiently low (e.g., < 3%; Franke et al., 2007). The domain dimensions and the computational grid were based on best practice guidelines (Casey and Wintergerste, 2000), on the recent single-sphere CFD study of Dixon et al. (2011) and on domain-size and grid-sensitivity analysis performed by the authors. The importance of appropriate grid development was recently indicated by Dixon et al. (2011), but in most CFD studies characteristics of the grid are not specified in detail. The LRNM grid is a hybrid grid (hexahedral, tetrahedral and prismatic cells) and consist of 2.8×10^6 cells. The grid is shown in Figure 2. On the surface of the sphere, in the boundary-layer region, 8 layers of prismatic cells were placed, with a distance (normal) from the cell centre point P of the wall-adjacent cell to the wall $y_P = 2.5 \times 10^{-5}$ m and an expansion ration of 1.3. On these layers of prismatic cells, tetrahedral cells were placed, and their size increased with distance from the sphere, with a maximal size of about 3.75×10^{-3} m (D/20) downstream of the sphere. These tetrahedral cells were applied in a square box (box size 3D) around the sphere (see Figure 2). Outside of this box, hexahedral cells were used. The spatial discretisation error was estimated by means of Richardson extrapolation (Franke et al., 2007; Roache, 1994), and is about 1% for both drag

force and convective heat transfer coefficient (CHTC [W $m^{-2}K^{-1}$]). These parameters were relevant for the subsequent analysis (see section 3). Grid convergence was monotonic. The grids were generated with ANSYS Gambit 2.4.6 software.

The reason for the high number of cells for such a simple flow problem is that the grid was designed to be used for LRNM. In order to resolve the boundary layer appropriately, grids constructed to be employed with LRNM require a high grid resolution (cell density) in the wall-normal direction, especially at high Reynolds numbers: the y^+ value in the wall-adjacent cell centre point P (y_P^+) should be about 1, which is much smaller compared to the requirements for WFs ($30 < y_P^+ < 500$). Here, y_P^+ is defined as $(\tau_w/\rho)^{1/2}y_P/\nu$, where ρ is the air density (1.225 kg m^{-3}), ν is the kinematic viscosity of air ($1.461\text{x}10^{-5}$ m^2 s^{-1}) and τ_w is the shear stress at the wall [Pa]. As τ_w increases with the Reynolds number, y_P has to decrease in order to maintain a y_P^+ of about 1. In this study, the highest y_P^+ values are below 1 for all evaluated air speeds. Another reason for the high number of cells is that very small triangular computational cells with a quasi uniform size were used on the sphere surface (surface area $\approx 1.0\text{x}10^{-7}$ m^2, hydraulic diameter $\approx 2.9\text{x}10^{-4}$ m, which is defined as four times the cross-sectional area of the cell, divided by its perimeter), as the grid was originally designed for a previous study (Defraeye et al., 2012a) to model microscopic scalar sources (e.g., lenticels or droplets) on the sphere surface. The small scale of these surface cells thus resulted in a high number of computational cells on the sphere surface ($4.1\text{x}10^4$ cells on ¼ sphere). Note that the influence of the cell size on the sphere surface will be addressed in section 3.4.

In addition to the LRNM grid, a grid for wall-function modelling was also designed. The wall-function grid had the same cell density as the LRNM grid outside the near-wall region, but in the near-wall region the grid was adapted in order to provide a higher y_P^+ value for the wall-adjacent cells. This resulted in a grid of about $1.8\text{x}10^6$ cells. On the surface of the sphere, in the boundary-layer region, one layer of prismatic cells was placed, with $y_P = 1.25\text{x}10^{-3}$ m. This resulted in y_P^+ values of about 40 (average value over sphere) at the highest Reynolds number ($3.2\text{x}10^4$). Although this value lies within the typical range for WFs ($30 < y_P^+ < 500$) at this air speed, y_P^+ values will become much less at lower air speeds, implying that larger cell wall distances (y_P) should be used. Larger y_P were however found to compromise the numerical stability of the simulation. Note that in most existing CFD codes, WFs are actually expressed as a function of the dimensionless y_P^* value, instead of the y_P^+ value, in order to deal with non-equilibrium boundary layers. This y_P^* value is a function of the turbulent kinetic energy, instead of the shear stress at the wall. In this study, the average y_P^+ and y_P^* values were very similar but their distribution over the sphere was clearly different, as already previously reported (Defraeye et al., 2010).

At the inlet of the domain, a uniform, low-turbulent velocity was imposed (see Figure 1). Free-stream air speeds (U_{ref}) of 0.002-6.325 m s^{-1} were evaluated, namely 0.002, 0.006325, 0.02, 0.06325, 0.2, 0.6325, 2 and 6.325 m s^{-1}. Subsequent speeds thus differ with a factor $10^{0.5}$, e.g., $6.325 = 2\text{x}10^{0.5}$. These speeds result in Reynolds numbers of 10 to $3.2\text{x}10^4$ ($Re = U_{ref}D/\nu$). This range of air speeds covers those typically found in storage rooms (about 0-1 m s^{-1}, e.g., Delele et al., 2009), as well as those found in pre-coolers, blast freezers, dryers and other types of processing equipment. The turbulence intensity (TI_{ref}) at the inlet was taken 0.1%, which was low and typical for most low-turbulence wind tunnels, allowing comparison with such experiments (see section 3). The specific dissipation rate (ω [s^{-1}]) was determined from $\omega = k^{1/2}/(0.07C_\mu^{1/4}L)$ (Fluent 12, 2009), where k is the turbulent kinetic energy [m^2 s^{-2}], $C_\mu = 0.09$ and L is a length scale

which is taken small (arbitrarily) and equal to $D/10$ [m]. The turbulence dissipation rate (ε [m^2 s^{-3}]) was determined from $\varepsilon = C_\mu^{3/4} k^{3/2}/(0.07L)$ (Fluent 12, 2009). The effect of turbulence inlet properties has been a subject of research (Ghisalberti and Kondjoyan, 1999; Kondjoyan, 2006; Peyrin and Kondjoyan, 2002), but an analysis of the impact of these variables was, although feasible with CFD, outside of the scope of the present study. Zero static pressure was imposed at the outlet, which is often used in similar studies (e.g., Dixon et al., 2011) and is advised in best practice guidelines (e.g., Franke et al., 2007). Symmetry boundary conditions were used for the lateral boundaries which assume that the normal velocity component and the normal gradients at the boundary are zero. The sphere surfaces were modelled as no-slip walls with zero roughness since surface roughness values cannot be specified if LRNM is used (Fluent 12, 2009).

Heat was taken as the (passive) scalar to study convective transport, implying, amongst others, no dependency of air density on the temperature. Note that heat and mass transport behave quasi analogous under specific conditions (amongst others, similar boundary conditions, no radiation, no coupling between heat and mass transfer, etc.). Under these conditions, the heat and mass transfer analogy can be applied to estimate convective mass transfer coefficients (CMTCs) out of CHTC data (e.g., see Defraeye et al., 2012b). The findings of this study for heat transfer can thus be transposed to mass transfer, for some cases. Note that aforementioned air properties were assumed constant, where the thermal conductivity of air (λ) in this study was prescribed to be 0.0242 W $m^{-1}K^{-1}$. A temperature of 10°C (T_{ref}) was imposed at the inlet of the computational domain. A uniform, higher temperature (T_w) of 20°C was imposed at the sphere surface, to allow a comparison with empirical Nusselt number data (see section 3).

2.2 Numerical simulation

The simulations were performed with the commercial CFD code ANSYS Fluent 12, which uses the control volume method. Several steady RANS turbulence models were evaluated for the sphere. These turbulence models were combined with boundary-layer modelling approaches (LRNM and WFs) to account for the influence of the wall. All evaluated turbulence models and boundary-layer modelling approaches are presented in detail in Table 1, and a brief background on them is given below.

Essentially, three types of turbulence models were evaluated: k-ε models, k-ω models and the Reynolds stress model (RSM). The k-ε and k-ω models are both eddy-viscosity models, which assume isotropic behaviour of turbulence, and which solve two additional turbulence transport equations, namely for turbulent kinetic energy and for turbulence dissipation. The turbulent viscosity, used to determine the Reynolds stresses, is calculated by assuming a specific relation between the transported variables, such as the turbulent kinetic energy (k) and the turbulence dissipation rate (ε), which is determined (empirically or theoretically) for specific flow conditions. Thereby some models perform better in specific flows than others. There is however no universally valid turbulence model which performs well for all classes of flows (Casey and Wintergerste, 2000). The RSM is a more advanced turbulence model which does not use the eddy-viscosity concept but solves for all Reynolds stresses and for turbulence dissipation. This results in seven turbulence transport equations for three-dimensional flow problems, by which the RSM accounts for turbulence anisotropy, i.e. directional effects in the Reynolds stress field. Thereby, an increased accuracy can be obtained for complex flows but the numerical stability, i.e. convergence behaviour, is however more critical and the computational

cost increases. More details of these turbulence models can be found in the referred publications and their performance is clearly discussed in Casey and Wintergerste (2000) or Pope (2009).

When turbulence models are combined with LRNM, the entire boundary layer is resolved explicitly by discretising (meshing) the computational domain in the boundary layer at a very high (grid) resolution. The k-ω models account for damping of turbulence in the vicinity of the wall themselves. The k-ε models and RSM, originally developed as high-Reynolds number models, however require the use of additional damping functions. For such low-Reynolds number modifications, a two-layer approach was used: turbulence in the turbulent core region of the flow was resolved by the turbulence model, and the one-equation LRNM Wolfshtein model (Wolfshtein, 1969) was used to resolve turbulence in the viscosity-affected region, and accounted for damping of turbulence. Note that this one-equation low-Reynolds number model is less complex than the two-equation k-ω models, which are in essence developed to deal with near-wall (low-Reynolds number) flows: the Wolfshtein model only solves one transport equation for turbulence instead of two, which can lead to a reduced performance. An interesting modification to the standard k-ω model was proposed by Menter (1994): the shear stress transport (SST) k-ω model. This model uses a two-equation k-ω model formulation to solve the near-wall region, for which the k-ω models were originally developed, while a k-ε model formulation, developed for high-Reynolds number flows, is used to solve the turbulent core region of the flow. This model can improve flow predictions with strong non-equilibrium effects and retains the k-ω model near-wall performance (Casey and Wintergerste, 2000), by which it seems very suitable for the present study.

When turbulence models are combined with WFs, the flow quantities in the boundary-layer region are modelled by functions, instead of resolving the boundary layer explicitly. This facilitates grid generation and increases computational economy but can lead to inaccurate predictions, particularly of wall friction and convective heat transfer (e.g., Defraeye et al., 2010a). The standard formulation (Launder and Spalding, 1974), referred to as standard wall functions (SWFs), was used to model the flow quantities (velocity, temperature, turbulence) in the logarithmic layer for both the standard k-ε model and the SST k-ω model. These specific turbulence models were chosen since the standard k-ε model is still the most commonly used model in CFD engineering (Casey and Wintergerste, 2000) and the SST k-ω model is expected to have a good performance with LRNM, by which comparing its performance with WFs could be interesting. Details on the WFs implementation can be found in Fluent 12 (2009). To ensure the validity of the WFs throughout the entire boundary layer (viscous sublayer, buffer layer and logarithmic layer), blending functions between these layers were included (Fluent 12, 2009).

Furthermore, second-order discretisation schemes were used throughout. The SIMPLE algorithm was used for pressure-velocity coupling. Pressure interpolation was second order. Buoyancy effects were not taken into account in the simulations since the focus of this paper was on passive scalar transport. In this case, the flow field is independent of the imposed scalar (thermal) boundary conditions, which implies forced convective flow and passive scalar (heat) transfer. Thereby, the reported results are more generally useable and are also applicable for transport of other scalars, such as water vapour. Note that not accounting for buoyancy also allowed to specify larger temperature differences between the sphere surface and the air flow, which avoids numerical round-off errors related to very small temperature differences. Radiation was not considered in the simulations since a constant temperature was imposed at the sphere surface and since the heat and mass transfer analogy is not valid if radiation is accounted for. Iterative convergence of the numerical

simulation was assessed by monitoring the velocity, turbulent kinetic energy and temperature on specific locations in the flow field, namely where large gradients are found (i.e., in the recirculation zone), and the drag force and heat fluxes (surface-averaged value) of the sphere. The iterative procedure was stopped when these parameters became quasi constant with subsequent iterations.

3. Results and discussion

3.1 Empirical data

The accuracy of CFD simulations of flow and scalar transfer around a sphere is assessed at several Reynolds numbers by comparison of different parameters with empirical data. These parameters are well established for spheres in several textbooks (e.g., Clift et al., 1978): (1) drag coefficient $C_D = F_d/(0.5\rho U_{ref}^2 A_f)$, where F_d is the drag force [N] and A_f is the frontal area [m²]; (2) Nusselt number Nu = CHTC.D/λ; (3) separation angle (θ_s [°]), which is defined as the angle at which the shear stress at the wall becomes quasi equal to zero (e.g., see Dixon et al., 2011) . This angle is taken zero at the windward stagnation point; (4) recirculation length (L_r [m]), which is defined as the (maximal) downstream distance from the sphere where the streamwise velocity component (x-direction in Figure 1) becomes zero.

The following empirical functions of C_D (from Clift et al., 1978), Nu (from Whitaker, 1972) and θ_s (from Clift et al., 1978) for flow around a sphere are used for comparison with CFD simulations.

$$C_D = \begin{cases} (24/\mathrm{Re})\left(1+0.1315\,\mathrm{Re}^{0.82-0.05\log \mathrm{Re}}\right) & \text{for } 0.01<\mathrm{Re}<20 \\ (24/\mathrm{Re})\left(1+0.1935\,\mathrm{Re}^{0.6305}\right) & \text{for } 20<\mathrm{Re}<260 \\ 10^{1.6435-1.1242\log \mathrm{Re}+0.1558(\log \mathrm{Re})^2} & \text{for } 260<\mathrm{Re}<1500 \\ 10^{-2.4571+2.5558\log \mathrm{Re}-0.9295(\log \mathrm{Re})^2+0.1049(\log \mathrm{Re})^3} & \text{for } 1500<\mathrm{Re}<12000 \\ 10^{-1.9181+0.637\log \mathrm{Re}-0.0636(\log \mathrm{Re})^2} & \text{for } 12000<\mathrm{Re}<44000 \end{cases} \quad (1)$$

$$\mathrm{Nu} = 2+\left(0.4\,\mathrm{Re}^{0.5}+0.06\,\mathrm{Re}^{0.667}\right)\mathrm{Pr}^{0.4}\left(\frac{\mu}{\mu_{\mathrm{wall}}}\right)^{0.25} \quad (2)$$

$$\theta_s = \begin{cases} 180-42.5\left[\ln\left(\mathrm{Re}/20\right)\right]^{0.438} & \text{for } 20<\mathrm{Re}<400 \\ 78+275\,\mathrm{Re}^{-0.37} & \text{for } 400<\mathrm{Re}<300000 \end{cases} \quad (3)$$

where μ and μ_{wall} are the absolute viscosities of the fluid and of the fluid at the wall, respectively ([kg m^{-1}s^{-1}]), which are equal in this study (see section 2.1) as air properties are assumed constant; Pr is the Prandtl number (= $c_p\mu/\lambda$), with c_p the specific heat capacity of air, taken equal to 1006.43 J kg^{-1}K^{-1}. For L_r, empirical data reported by Clift et al. (1978), Hucho (2011) and Jang and Lee (2008) is taken, where L_r is represented dimensionless by means of D. A distinct scatter on the data is present (see below), which can be related to the free-stream turbulence level, the sphere supporting method or different working fluids (Jang and Lee, 2008). Hence comparison with CFD results for L_r will not be as clear as with the other parameters.

3.2 Turbulence modelling

A comparison of empirical flow parameters (C_D, Nu, θ_s and L_r) with those obtained from CFD (for different RANS turbulence models, in combination with LRNM) is presented in Figure 3 as a function of the Reynolds number. Since a

logarithmic scale is used in Figure 3a and 3c, differences in C_D and Nu will appear less pronounced here. Therefore a focus on the high-Reynolds number region is presented in Figures 3b and 3d, i.e. without logarithmic scaling. For comparison of the flow field of different turbulence models, the streamlines for all models are presented in the centreplane of the sphere ($z = 0$ in Figure 1) for $Re = 10^4$ ($U_{ref} = 2$ m s^{-1}) in Figure 4.

Before comparing the turbulence models, note that all models perform well for Reynolds numbers below about 300, where flow was found to be essentially laminar. Discrepancies with empirical data are found at higher Reynolds numbers.

The performance of all k-ε models (sk-ε, rng k-ε, rk-ε) is very similar, for all parameters. Of all turbulence models, they show the largest discrepancies with empirical data, particularly at high Reynolds numbers. Nu and θ_s are overpredicted, L_r is strongly underpredicted and C_D does both. As seen in Figure 4, the predicted wake zone of these models is very small. This weak performance can be related both to the k-ε model itself as to LRNM, for which a one-equation model is used to model turbulence damping in the vicinity of the wall. Kondjoyan and Boisson (1997) showed that performance of such damping functions could be improved by fitting of the damping parameter.

RSM performs satisfactory for all flow parameters. L_r however strongly increases at higher Reynolds numbers, whereas it should remain rather constant. The good performance of RSM indicates that accounting for turbulence anisotropy can increase accuracy, compared to "isotropic" k-ε models, and that LRNM with the one-equation model is not (only) to blame for the weak performance of the k-ε models. RSM however requires solving more transport equations (7 instead of 2), hence an increased computational cost, and convergence stability is usually less.

The performance of the k-ω models is much better than the other two-equation (i.e., k-ε) models, and they are known to perform better for boundary layers with strong pressure gradients (Casey and Wintergerste, 2000; Pope, 2009). The standard k-ω model performs well for C_D, Nu and θ_s but L_r is quite high. The SST k-ω model performs very well for all parameters over the entire Reynolds number range, but some discrepancies are found for C_D at the highest Reynolds numbers (< 15%). The good performance of the SST k-ω model (Menter, 1994) is related to the fact that it uses a two-equation k-ω model formulation to solve the near-wall region, for which the k-ω model was originally developed, whereas a k-ε model formulation is used to solve the turbulent core region of the flow, such as the wake zone. In the SST k-ω model, the sensitivity to the imposed free-stream value of ω, present in the standard k-ω model, is also eliminated (Casey and Wintergerste, 2000). Other studies also reported a good performance of the SST k-ω model for flow around streamlined bluff bodies (amongst others, Defraeye et al., 2010b; Dixon et al., 2011). The agreement of the SST k-ω model for C_D is, however, significantly better than found by Dixon et al. (2011) (see Defraeye et al., 2012a for a comparison). Dixon et al. (2011) stated that the SST k-ω model was only acceptable as an engineering approximation for C_D predictions, but it was found to be sufficiently accurate for convective heat transfer predictions. The higher accuracy of C_D in the present study is attributed to the very high number of computational cells on the sphere surface (see section 2.1). The influence of this grid resolution will be investigated in detail in section 3.4.

Of all evaluated turbulence models, the SST k-ω model clearly shows the best performance, and its good agreement with empirical data (in general < 5%) is actually quite exceptional for steady RANS simulations. The results of this

CFD validation study indicate that the (LRNM) SST k-ω model can provide sufficient accuracy for flow and scalar transfer predictions for a single sphere, within an air speed (Reynolds number) range relevant for postharvest and food processing studies. It is however imperative that all grid requirements for LRNM are respected and that a grid sensitivity analysis is performed (see section 2.1). The performance of the SST k-ω model is assumed to be similar for spherically-shaped food products, such as an apple. Also for more complex configurations, e.g., stacks in which the sphere is the basic component, the performance of the SST k-ω model is expected to be good, and much better than other turbulence models, but further verification is required on this behalf. Note however that for low sphere Reynolds numbers (i.e., below about 300), other turbulence models also perform satisfactory since flow was essentially laminar. In some food engineering applications, e.g., products stacked in a container in a cool room, such low sphere Reynolds numbers can occur (inside the container). In such cases, the choice of the turbulence model should rather be based on optimising flow predictions outside of the containers.

3.3 Boundary-layer modelling

A comparison of the empirical flow parameters (C_D, Nu, θ_s and L_r) with those obtained from CFD (for different boundary-layer modelling approaches) is presented in Figure 5 as a function of the Reynolds number. The SST k-ω model and the standard k-ε model are evaluated both with LRNM and WF. The former since it performed the best of all turbulence models (section 3.2) and the latter since it is (in combination with WFs) still the most commonly used model in CFD engineering (Casey and Wintergerste, 2000). For comparison of the flow field of different models, the streamlines for all models are presented in the centreplane of the sphere (z = 0 in Figure 1) for $Re = 10^4$ (U_{ref} = 2 m s^{-1}) in Figure 6.

Again, discrepancies with empirical data are mainly found at higher Reynolds numbers. The performance of the standard k-ε model was already not good in combination with LRNM, but it even becomes worse when using WFs. Especially θ_s is strongly overpredicted at high Reynolds numbers, resulting in an even smaller wake zone. Also large discrepancies are found for Nu (up to 40%), thus for the CHTC, which is often an important parameter for food engineering applications, and differences up to 60% are found for C_D. The accuracy of the SST k-ω model strongly decreases when using WFs, and shows many similarities with the standard k-ε model with WFs, i.e., an overprediction of Nu and θ_s, an underprediction of L_r, and both for C_D. Applying WFs is found to reduce the accuracy more than any turbulence model used with LRNM.

For rather streamlined bluff bodies such as spheres, the boundary-layer modelling approach has a large impact on the resulting flow field around the body, as it determines, in part, the location the boundary-layer separation points. SWFs are derived for wall-attached boundary layers under so-called equilibrium conditions, i.e., small pressure gradients, local equilibrium between generation and dissipation of turbulent energy and a constant (uniform) shear stress and heat flux in the near-wall region (Casey and Wintergerste, 2000). This wall-function concept breaks down for more complex flows, such as flow around bluff bodies where the boundary layer does not remain attached to the surface anymore, which is clearly confirmed in this study. LRNM, on the other hand, requires a very fine grid in the near-wall region, which is often not practically feasible for complex 3D configurations (Kondjoyan, 2006), with respect to computational economy and grid generation. Especially in stacks of spheres, it will be difficult to obtain a y_P^+ value equal to 1: providing cells with the required, small cell wall distance (y_P) by using prismatic cells on the sphere surface will be not

straightforward, or possible. As a result, CHTC predictions are sometimes argued to be unreliable for such configurations as WFs have to be applied (Kondjoyan, 2006).

3.4 Grid cell density on sphere surface

As mentioned, the computational grid was constructed based on a grid sensitivity analysis. The size of the (2D) triangular computational cells on the sphere surface was, however, chosen very small to allow modelling of microscopic scalar sources in a previous study (see section 2.1). This small cell size was argued to be a possible reason for the very good performance of the (LRNM) SST k-ω model (see section 3.2), compared to the study of Dixon et al. (2011). For realistic configurations in food engineering, e.g., many products stacked in a container, such a small cell size on the surface is not feasible, and larger cells on the product surface are used. A lower spatial resolution can however influence the flow-field predictions, as boundary-layer modelling is very critical for spherical products. To investigate the influence of cell size/density on the sphere surface, four different grids were evaluated. These grids were built up the same way and only differ in the amount of 2D triangular cells on the sphere surface. In Figure 7, these grids (Grid 1-4) are presented and in Table 2 information on these grids is given. Grid 1 is the reference grid, used in previous simulations (section 3.2-3.3) and the subsequent grids all have a lower cell density on the sphere surface. The coarsest grid (Grid 4) has a cell size typically used in food engineering applications (i.e., a few mm). Note that these grids (Grids 2-4) were not used for the grid sensitivity analysis (see section 2.1), as the grid density in the entire computational domain was different for the grids used there. For the grids investigated in the present section (Grids 1-4), only the cell density on the sphere surface was different.

A comparison of the empirical flow parameters (C_D, Nu, θ_s and L_r) with those obtained from CFD (for different cell densities on the sphere surface, using the SST k-ω model with LRNM) is presented in Figure 8 as a function of the Reynolds number. A clear trend towards larger discrepancies with empirical data is found for lower cell densities on the sphere surface. Although still more accurate than other turbulence models with LRNM (see section 3.2), the results from the coarsest grid (Grid 4) are much less reliable. Particularly interesting is that the total amount of (3D) cells in the computational domain strongly decreases with increasing (2D) cell size on the sphere surface between Grid 1 and Grid 2, whereas the subsequent decrease is much less when comparing Grid 2 with Grid 4. Since the performance of Grid 2, compared to Grid 1, is still very satisfactory, this means that an optimal cell size on the sphere surface can be determined which provides sufficient accuracy at an acceptable computational cost. Grid 2 has a characteristic cell size of about 0.6 mm (i.e., the hydraulic diameter).

5. Conclusions

In this study, several RANS turbulence models and boundary-layer modelling approaches were compared with empirical data for flow and scalar transfer around a single sphere for a sphere Reynolds number range relevant for postharvest and food processing applications, namely Re = 10 to 3.2×10^4. With respect to turbulence modelling, in combination with low-Reynolds number modelling (LRNM) of the boundary layer, the k-ε models did not perform well, particularly at high Reynolds numbers. The Reynolds stress model and the standard k-ω model performed satisfactory. The shear stress transport (SST) k-ω model showed a very good performance for all evaluated flow parameters (drag coefficient, Nusselt number, separation angle and recirculation length), generally with errors below 5%, which is quite exceptional for steady RANS. Its performance confirms that the turbulence model characteristics

(when combined with LRNM) are particularly suitable to deal with this specific flow problem, i.e. non-equilibrium flow where (low-Reynolds number) modeling of the boundary layer is important. With respect to boundary-layer modelling, standard wall functions (WFs) resulted in inaccurate predictions, compared to LRNM, and should be avoided. This however conflicts with CFD modelling of complex configurations, where LRNM grids and their inherently higher computational cost are often not practically feasible, leaving WFs as the only option. Furthermore, the influence of the cell size/density on the sphere surface was investigated. It was shown that using cell sizes on the sphere surface, typical for CFD studies in food engineering (a few mm), can compromise the accuracy of the SST k-ω model (with LRNM), as actually grids with much smaller cell sizes are required.

In CFD simulations for spheres, and especially for stacks of spheres, an important compromise will have to be made between numerical accuracy on the one hand, and computational cost and ease of grid generation on the other hand. Typically, unsteady methods (unsteady RANS or large-eddy simulation) and LRNM require a higher computational cost and more strict grid requirements, but can improve accuracy compared to some steady RANS turbulence models, used in combination with WFs.

In this CFD validation study, a systematic comparison of the performance of the most readily available turbulence models and boundary-layer modelling approaches in commercial CFD packages was presented for a single sphere, by comparing different parameters related to flow and scalar transfer. The results are of use for CFD researchers and practitioners in the field of postharvest and food process engineering with spherical foods.

Acknowledgements

Thijs Defraeye is a postdoctoral fellow of the Research Foundation – Flanders (FWO) and acknowledges its support. Financial support by the Research Foundation – Flanders (project FWO G.0603.08) and KU Leuven (project OT 08/023) is also gratefully acknowledged. These sponsors had no involvement in: the study design, the collection, analysis and interpretation of data; the writing of the manuscript; and the decision to submit the manuscript for publication.

References

Ambaw, A., Delele, M., Defraeye, T., Ho, Q.T., Opara, U.L., Nicolai, B., & Verboven, P. (2012a). The use of CFD to characterize and design post-harvest storage facilities: Past, present and future. *Computers and Electronics in Agriculture*, Accepted.

Ambaw, A., Verboven, P., Delele, M.A., Defraeye, T., Tijskens, E., Shenk, A., & Nicolai, B. (2012b). CFD modelling of the 3D spatial and temporal distribution of 1-methylcyclopropene in apple fruit storage. *Food and Bioprocess Technology*, In press (doi:10.1007/s11947-012-0913-7).

Casey, M., & Wintergerste, T. (2000). *ERCOFTAC Special Interest Group on "Quality and Trust in Industrial CFD": Best Practice Guidelines*, ERCOFTAC.

Clift, R., Grace, J.R., & Weber, M.E. (1978). *Bubbles, drops and particles* (1st ed.). Dover Publications Inc., New York, USA.

Constantinescu, G., & Squires, K. (2004). Numerical investigations of flow over a sphere in the subcritical and supercritical regimes. *Physics of Fluids*, 16(5), 1449-1466.

da Silva, W.P., e Silva, C.M.D.P.S., Farias, O.V.S., & e Silva, D.D.P.S. (2010). Calculation of the convective heat transfer coefficient and cooling kinetics of an individual fig fruit. *Heat and Mass Transfer*, 46(3), 371-380.

Defraeye, T., Blocken, B., & Carmeliet, J. (2010a). CFD analysis of convective heat transfer at the surfaces of a cube immersed in a turbulent boundary layer. *International Journal of Heat and Mass Transfer*, 53(1-3), 297-308.

Defraeye, T., Blocken, B., Koninckx, E., Hespel, P., & Carmeliet, J. (2010b). Computational fluid dynamics analysis of cyclist aerodynamics: Performance of different turbulence-modelling and boundary-layer modelling approaches. *Journal of Biomechanics*, 43(12), 2281-2287.

Defraeye, T., Herremans, E., Verboven, P., Carmeliet, J., & Nicolai, B. (2012a). Convective heat and mass exchange at surfaces of horticultural products: a microscale CFD modelling approach. *Agricultural and Forest Meteorology*, 162-163, 71-84.

Defraeye, T., Blocken, B., & Carmeliet, J. (2012b). Analysis of convective heat and mass transfer coefficients for convective drying of a porous flat plate by conjugate modelling, *International Journal of Heat and Mass Transfer*, 55(1-3), 112-124.

Dehghannya, J., Ngadi, M., & Vigneault, C. (2010). Mathematical modeling procedures for airflow, heat and mass transfer during forced convection cooling of produce: A review. *Food Engineering Reviews*, 2(4), 227-243.

Delele, M., Tijskens, E., Atalay, Y.T., Ho, Q.T., Ramon, H., Nicolai, B., & Verboven, P. (2008). Combined discrete element and CFD modelling of airflow through random stacking of horticultural products in vented boxes. *Journal of Food Engineering*, 89(1), 33-41.

Delele, M., Schenk, A., Tijskens, E., Ramon, H., Nicolai, B., & Verboven, P. (2009). Optimization of the humidification of cold stores by pressurized water atomizers based on a multiscale CFD model. *Journal of Food Engineering*, 91(2), 228-239.

Dhole, S.D., Chhabra, R.P., & Eswaran, V. (2006). A numerical study on the forced convection heat transfer from an isothermal and isoflux sphere in the steady symmetric flow regime. *International Journal of Heat and Mass Transfer*, 49(5-6), 984-994.

Dixon, A.G., Taskin, M.E., Nijemeisland, M., & Stitt, E.H. (2011). Systematic mesh development for 3D CFD simulation of fixed beds: Single sphere study. *Computers & Chemical Engineering*, 35(7), 1171-1185.

Feng, Z.G., & Michaelides, E.E. (2000). A numerical study on the transient heat transfer from a sphere at high Reynolds and Peclet numbers. *International Journal of Heat and Mass Transfer*, 43(2), 219-229.

Fluent 12 (2009). *Ansys Fluent 12.0 User's Guide*. Ansys Inc.

Franke, J., Hellsten, A., Schlünzen, H., & Carissimo, B. (2007). *Best practice guideline for the CFD simulation of flows in the urban environment*. COST Action 732: Quality assurance and improvement of microscale meteorological models, Hamburg, Germany.

Ghisalberti, L, & Kondjoyan, A. (1999). Convective heat transfer coefficients between air flow and a short cylinder. Effect of air velocity and turbulence. Effect of body shape, dimensions and position in the flow. *Journal of Food Engineering*, 42(1), 33-44.

Hoang, M., Verboven, P., De Baerdemaeker, J., & Nicolai, B. (2000). Analysis of the air flow in a cold store by means of computational fluid dynamics. *International Journal of Refrigeration*, 23(2), 127-140.

Hoang, M., Verboven, P., Baelmans, M., & Nicolaï, B. (2003). A continuum model for airflow, heat and mass transfer in bulk of chicory roots. *Transactions of the ASAE*, 46(6), 1603-1611.

Hu, Z., & Sun, D.-W. (2001). Predicting the local surface heat transfer coefficients by different turbulent k-ε models to simulate heat and moisture transfer during air-blast chilling. *International Journal of Refrigeration*, 24(7), 702-717.

Hucho, W.-H. (2011). *Aerodynamik der stumpfen Körper* (2nd ed.), Viewig + Teubner Verlag, Wiesbaden, Germany.

Jang, Y.I., & Lee, S.J. (2008). PIV analysis of near-wake behind a sphere at a subcritical Reynolds number. *Experiments in Fluids*, 44(6), 905-914.

Johnson, T.A., & Patel, V.C. (1999). Flow past a sphere up to a Reynolds number of 300. *Journal of Fluid Mechanics*, 378, 19-70.

Jones, W.P., & Launder, B.E. (1972). The prediction of laminarization with a two-equation model of turbulence. *International Journal of Heat and Mass Transfer*, 15, 301-314.

Kaya, A., Aydin, O., & Dincer, I. (2006). Numerical modeling of heat and mass transfer during forced convection drying of rectangular moist objects. *International Journal of Heat and Mass Transfer*, 49(17-18), 3094-3103.

Kondjoyan, A. (2006). A review on surface heat and mass transfer coefficients during air chilling and storage of food products. *International Journal of Refrigeration*, 29(6), 863-875.

Kondjoyan, A., & Boisson, H.C. (1997). Comparison of calculated and experimental heat transfer coefficients at the surface of circular cylinders placed in a turbulent cross-flow of air. *Journal of Food Engineering*, 34(2), 123-143.

Launder, B.E. (1989). Second-moment closure and its use in modelling turbulent industrial flows. *International Journal for Numerical Methods in Fluids*, 9(8), 963-985.

Launder, B.E., & Spalding, D.B. (1974). The numerical computation of turbulent flows. *Computer Methods in Applied Mechanics and Engineering*, 3(2), 269-289.

Martins, M.A., Oliveira, L.S., & Saraz, J.A. (2011). Numerical study of apple cooling in tandem arrangement. *Dyna-Colombia*, 78(166), 158-165.

Menter, F.R. (1994). Two-equation eddy-viscosity turbulence models for engineering applications. *AIAA Journal*, 32(8), 1598-1605.

Nahor, H., Hoang, M., Verboven, P., Baelmans, M., & Nicolai, B. (2005). CFD model of the airflow, heat and mass transfer in cool stores. *International Journal of Refrigeration*, 28(3), 368-380.

Peyrin, F., & Kondjoyan, A. (2002). Effect of turbulent integral length scale on heat transfer around a circular cylinder placed cross to an air flow. *Experimental Thermal and Fluid Science*, 26(5), 455-460.

Peralta, J.M., Rubiolo, A.C., & Zorrilla, S.E. (2010). Mathematical modeling of the heat transfer and flow field of liquid refrigerants in a hydrofluidization system with a stationary sphere. *Journal of Food Engineering*, 99(3), 303-313.

Pope, S.B. (2009). *Turbulent Flows* (1st ed.). Cambridge University Press, Cambridge, UK.

Roache, P.J. (1994). Perspective: a method for uniform reporting of grid refinement studies. *Transactions of the ASME - Journal of Fluids Engineering*, 116(3), 405-413.

Shih, T.H., Liou, W.W., Shabbir, A., Yang, Z., & Zhu, J. (1995). A new k-ε eddy viscosity model for high Reynolds number turbulent flows. *Computers & Fluids*, 24(3), 227-238.

Tutar, M., Erdogdu, F., & Toka, B. (2009). Computational modeling of airflow patterns and heat transfer prediction through stacked layers' products in a vented box during cooling. *International Journal of Refrigeration*, 32(2), 295-306.

Verboven, P., Nicolai, B., Scheerlinck, N., & De Baerdemaeker, J. (1997). The local surface heat transfer coefficient in thermal food process calculations: a CFD approach. *Journal of Food Engineering*, 33(1-2), 15-35.

Verboven, P., Scheerlinck, N., De Baerdemaeker, J., & Nicolai, B. (2000a). Computational fluid dynamics modeling and validation of the temperature distribution in a forced convection oven. *Journal of Food Engineering*, 43(2), 61-73.

Verboven, P., Scheerlinck, N., De Baerdemaeker, J., & Nicolai, B. (2000b). Computational fluid dynamics modeling and validation of the isothermal airflow in a forced convection oven. *Journal of Food Engineering*, 43(1), 41-53.

Verboven, P., Datta, A.K., Anh, N.T., Scheerlinck, N., & Nicolai, B. (2003). Computation of airflow effects on heat and mass transfer in a microwave oven. *Journal of Food Engineering*, 59(2-3), 181-190.

Verboven, P., Flick, D., Nicolai, B., & Alvarez, G. (2006). Modelling transport phenomena in refrigerated food bulks, packages and stacks: basics and advances. *International Journal of Refrigeration*, 29(6), 985-997.

Whitaker, S. (1972). Forced convection heat transfer correlations for flow in pipes, past flat plates, single cylinders, single spheres, and for flow in packed beds and tube bundles. *AIChE Journal*, 18(2), 361-371.

Wilcox, D.C. (1998). *Turbulence modeling for CFD*. DCW Industries Inc., California, USA.

Wolfshtein, M. (1969). The velocity and temperature distribution in one-dimensional flow with turbulence augmentation and pressure gradient. *International Journal of Heat and Mass Transfer*, 12(3), 301-318.

Yakhot, V., Orszag, S.A., Thangam, S., Gatski, T.B., & Speziale, C.G. (1992). Development of turbulence models for shear flows by a double expansion technique. *Physics of Fluids A*, 4(7), 1510-1520.

Zou, Q., Opara, L.U., & McKibbin, R. (2006). A CFD modeling system for airflow and heat transfer in ventilated packaging for fresh foods: I. Initial analysis and development of mathematical models. *Journal of Food Engineering*, 77(4), 1037-1047.

Defraeye T., Verboven P., Nicolai B. (2013), CFD modelling of flow and scalar exchange of spherical food products: turbulence and boundary-layer modelling, *Journal of Food Engineering* 114 (4), 495-504. http://dx.doi.org/10.1016/j.jfoodeng.2012.09.003

Tables

Table 1. Evaluated RANS turbulence models and boundary-layer modelling approaches.

Name	Turbulence model	Boundary-layer modelling approach
sk-ε	standard k-ε model (Jones and Launder, 1972)	LRNM
rng k-ε	renormalisation group k-ε model (Yakhot et al., 1992)	LRNM
rk-ε	realizable k-ε model (Shih et al., 1995)	LRNM
RSM	Reynolds stress model (Launder, 1989)	LRNM
sk-ω	standard k-ω model (Wilcox, 1998)	LRNM
SST k-ω	shear stress transport k-ω model (Menter, 1994)	LRNM
sk-ε - WF	standard k-ε model (Jones and Launder, 1972)	WFs (Launder and Spalding, 1974)
SST k-ω - WF	shear stress transport k-ω model (Menter, 1994)	WFs (Launder and Spalding, 1974)

Table 2. Information on computational grids with different cell sizes on the sphere surface (¼ sphere). Grid 1 is the reference grid.

Name	Number of (2D) triangular cells on sphere surface	Hydraulic diameter cells (mm)	Number of 3D cells in computational domain
Grid 1	40,552	0.29	2,798,908
Grid 2	10,168	0.58	1,681,544
Grid 3	2,456	1.18	1,535,552
Grid 4	660	2.27	1,425,556

Defraeye T., Verboven P., Nicolai B. (2013), CFD modelling of flow and scalar exchange of spherical food products: turbulence and boundary-layer modelling, *Journal of Food Engineering* 114 (4), 495-504. http://dx.doi.org/10.1016/j.jfoodeng.2012.09.003

Figures

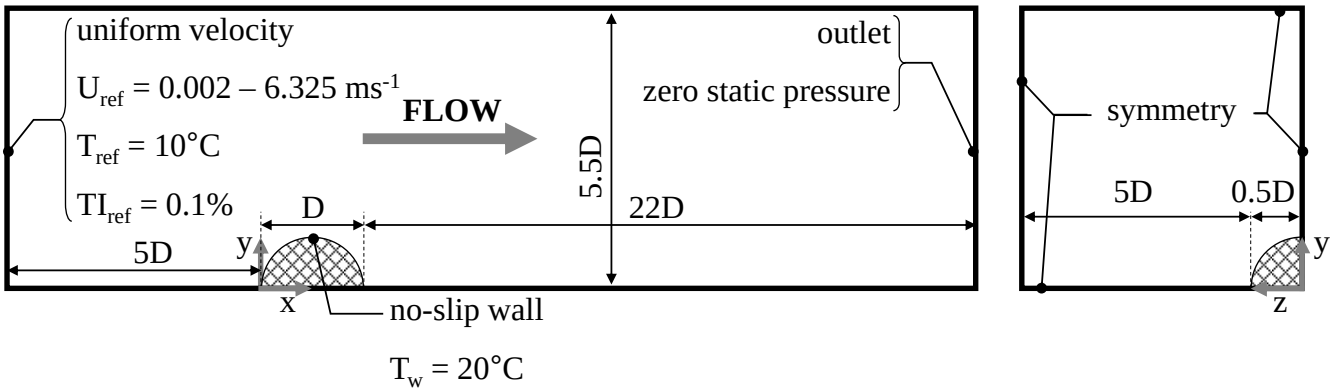

Figure 1. Computational domain (not to scale) and boundary conditions for the sphere model (¼ sphere, left: side view, right: frontal view).

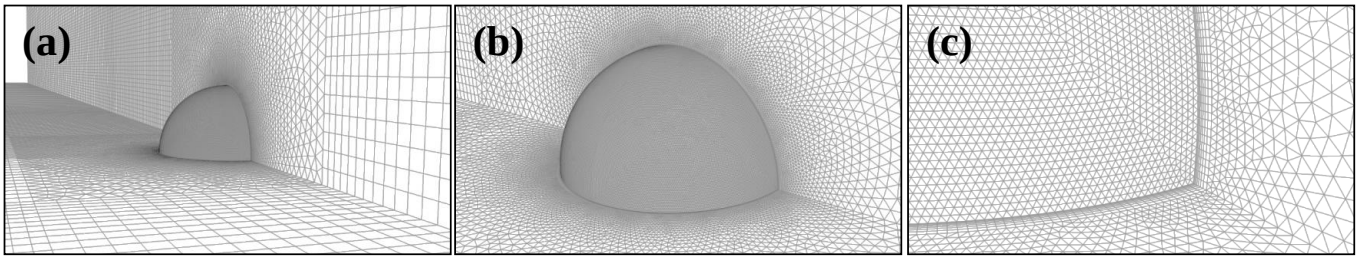

Figure 2. Computational grid for the sphere model (¼ sphere): (a) overview of computational domain including hexahedral cells; (b) grid around sphere with tetrahedral cells; (c) grid in boundary-layer region with prismatic cell layers on the sphere surface.

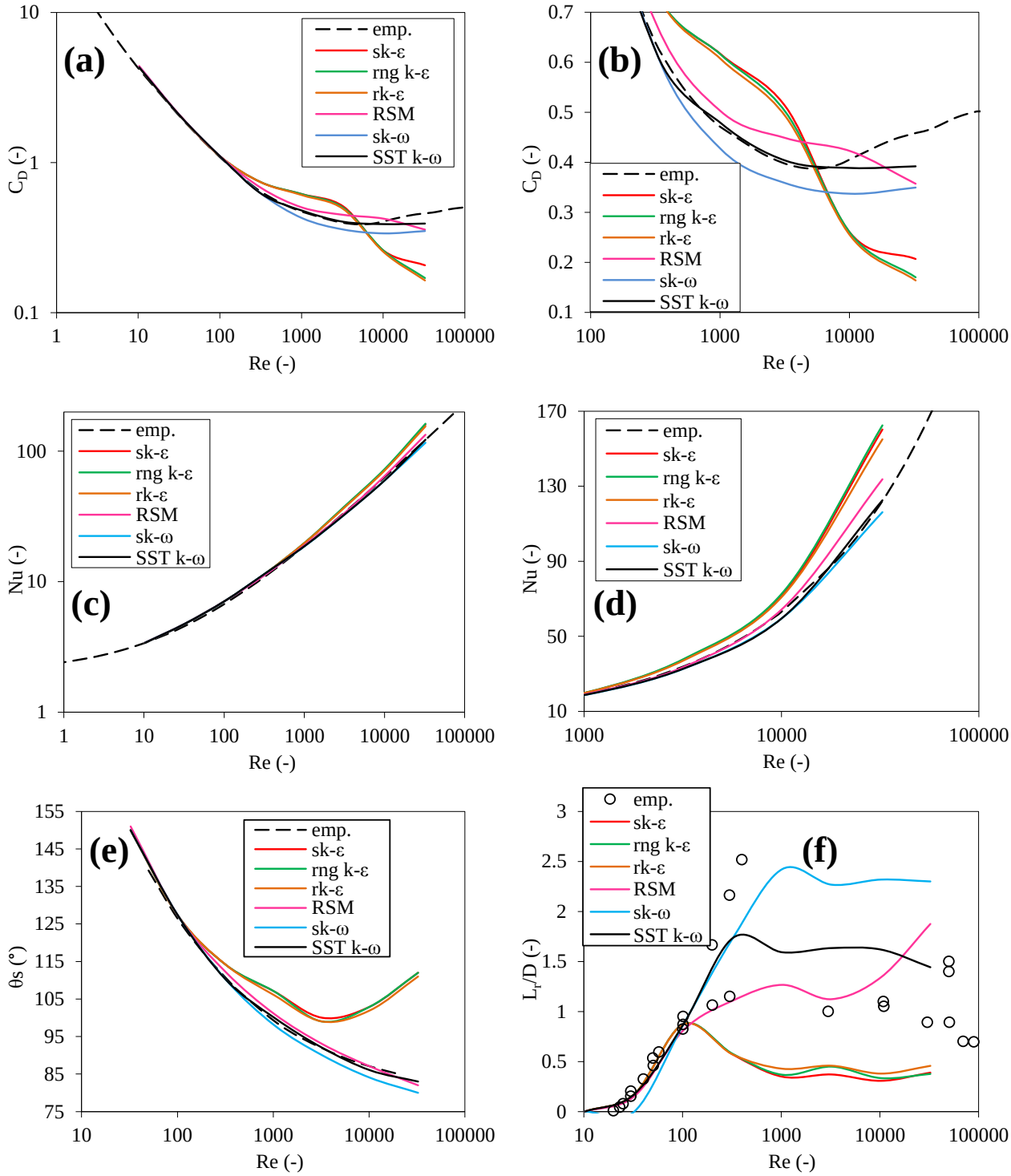

Figure 3. Comparison of CFD simulation data (different RANS turbulence models, with LRNM) with empirical sphere data (emp.), as a function of Reynolds number (logarithmic scale): (a-b) drag coefficient; (c-d) Nusselt number; (e) separation angle; (f) recirculation length, scaled with the sphere diameter. In (a) and (c) a vertical logarithmic scale is used.

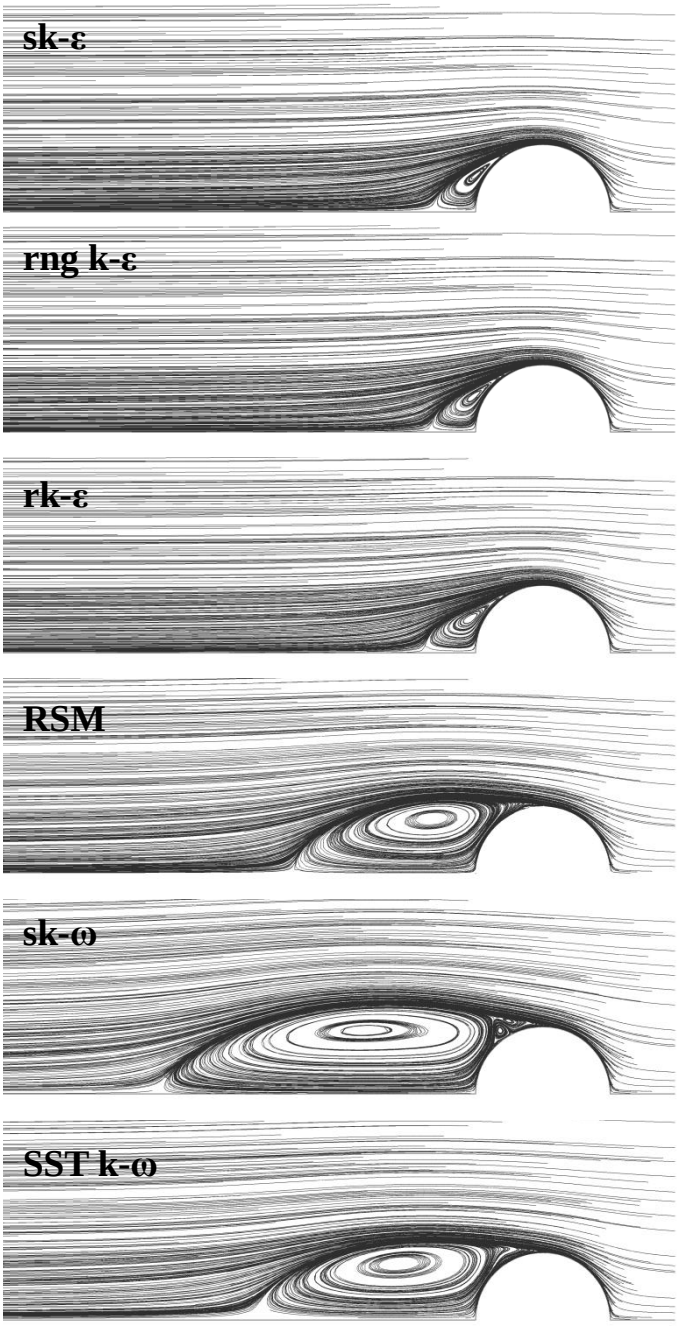

Figure 4. Streamlines around a sphere (side view) in the centreplane from CFD simulations with different RANS turbulence models (with LRNM) at a Reynolds number of 10^4 (U_{ref} = 2 m s^{-1}).

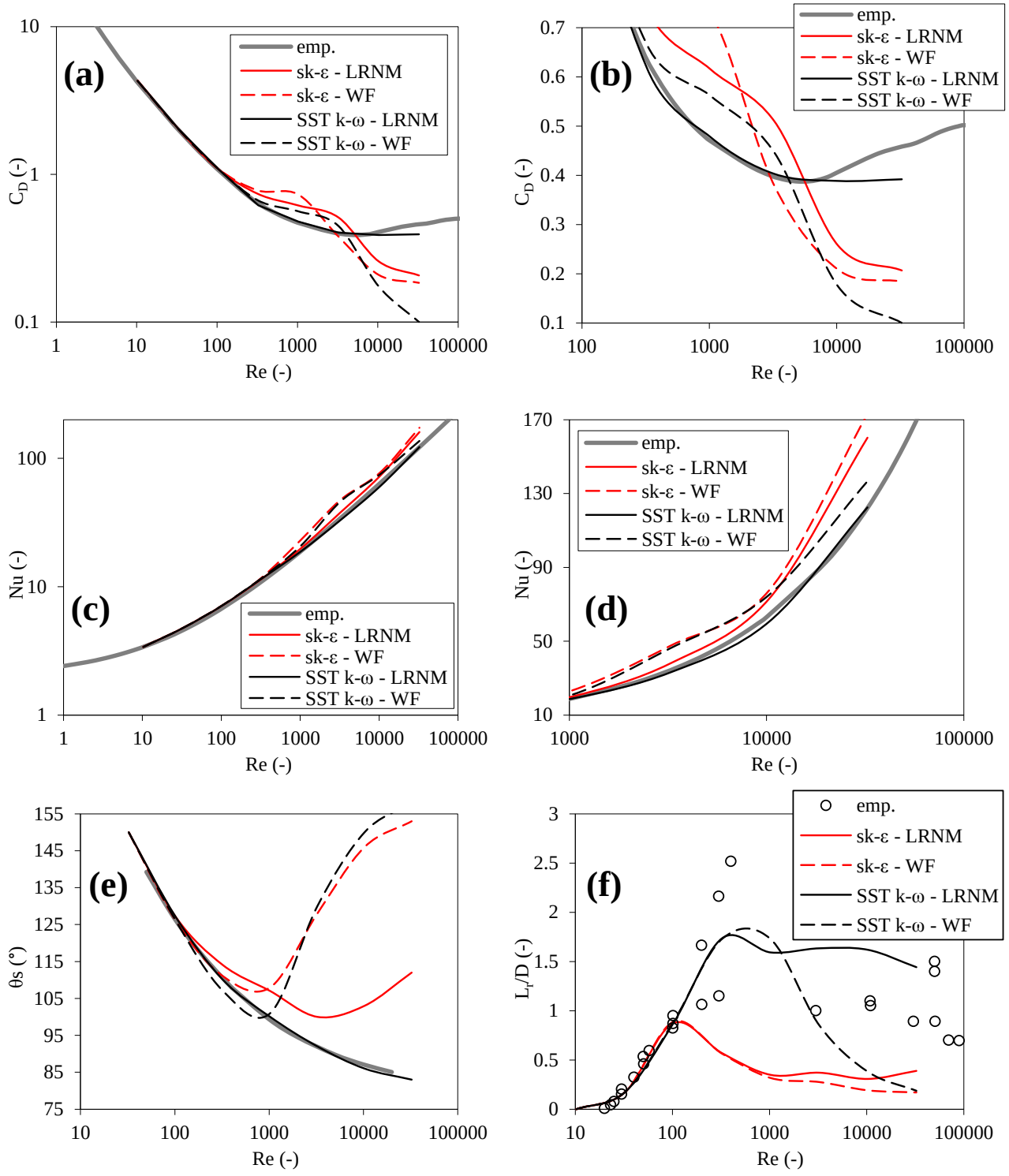

Figure 5. Comparison of CFD simulation data (different boundary-layer modelling approaches) with empirical sphere data (emp.), as a function of Reynolds number (logarithmic scale): (a-b) drag coefficient; (c-d) Nusselt number; (e) separation angle (the legend is not shown, but it is the same as in the other graphs); (f) recirculation length, scaled with the sphere diameter. In (a) and (c) a vertical logarithmic scale is used.

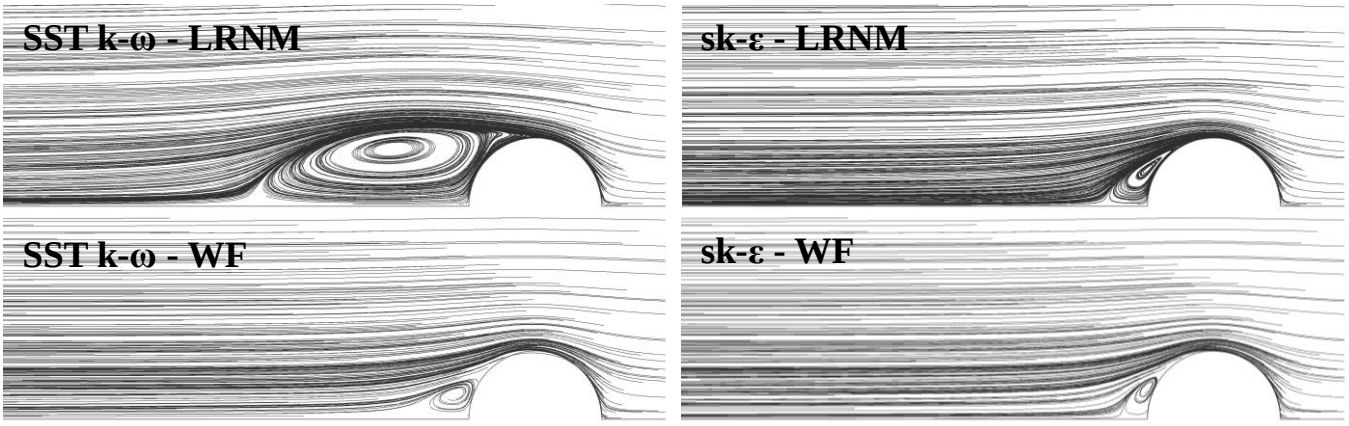

Figure 6. Streamlines around a sphere (side view) in the centreplane from CFD simulations with different boundary-layer modelling approaches at a Reynolds number of 10^4 (U_{ref} = 2 m s^{-1}).

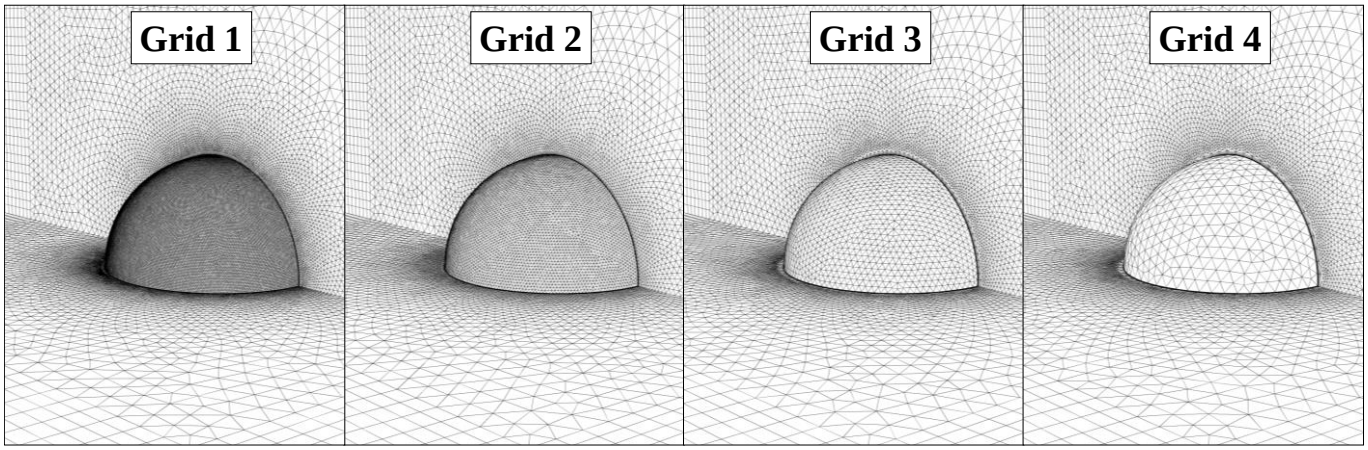

Figure 7. Computational grids with different cell sizes on the sphere surface (¼ sphere). Grid 1 is the reference grid.

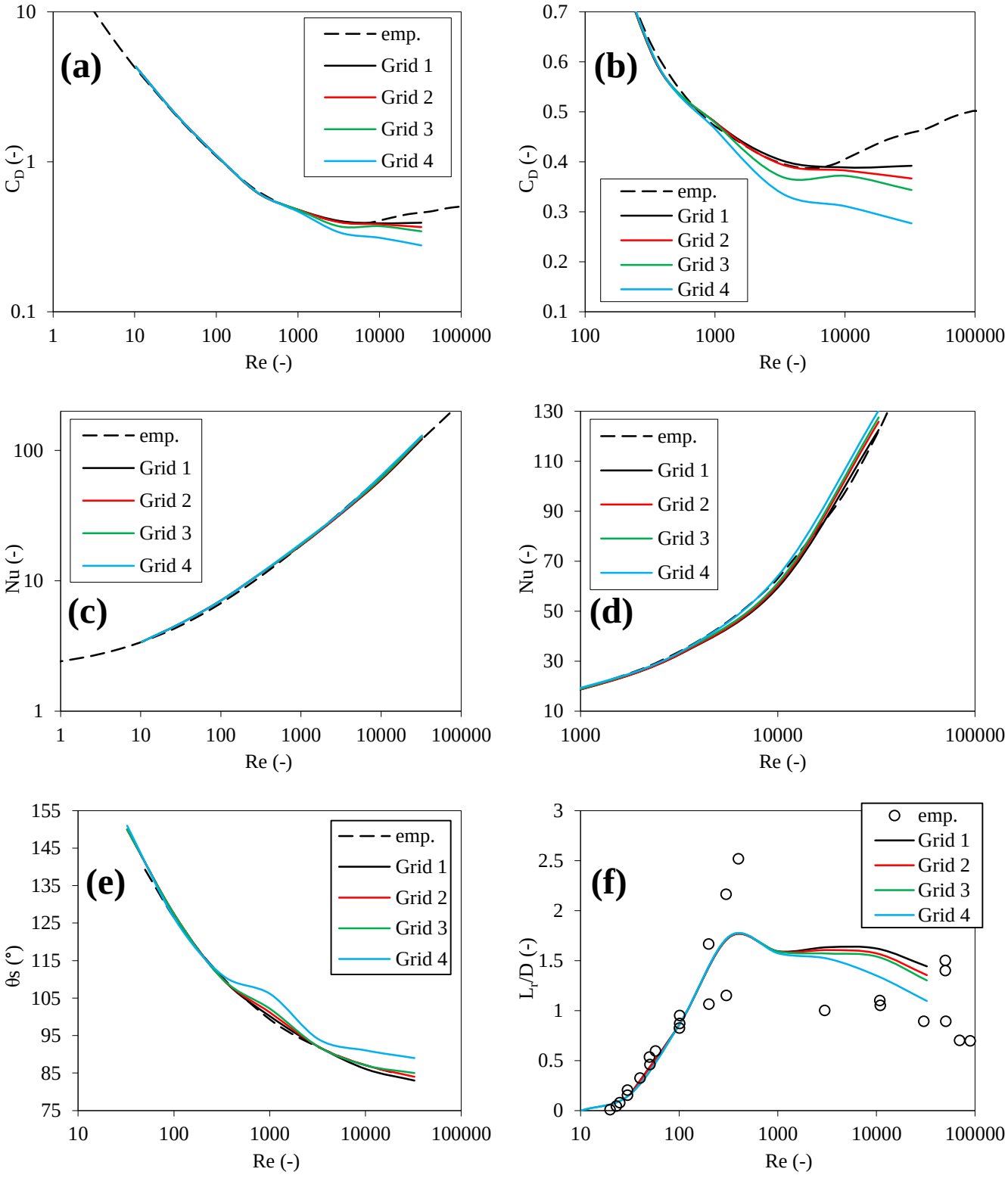

Figure 8. Comparison of CFD simulation data (different grid cell densities on sphere surface, SST k-ω model with LRNM) with empirical sphere data (emp.), as a function of Reynolds number (logarithmic scale): (a-b) drag coefficient; (c-d) Nusselt number; (e) separation angle; (f) recirculation length, scaled with the sphere diameter. In (a) and (c) a vertical logarithmic scale is used. Grid 1 is the reference grid.